CrossMark

## ORIGINAL ARTICLE

# Metabolomic study of the bone trabecula of osteonecrosis femoral head patients based on UPLC–MS/MS

Weiwen Zhu[1] · Tingmei Chen[2] · Shijia Ding[2] · Gang Yang[1] · Zhongwei Xu[1] ·
Kaimin Xu[1] · Shengyu Zhang[1] · Tao Ma[1] · Jian Zhang[1]

**Abstract** The severity and/or progression of osteonecrosis of the femoral head (ONFH) are commonly assessed by radiography, nuclear magnetic resonance image which aren't invariably correlated to severity of disease and may be disturbed by other factors. Consequently, exploring the novel biochemical signatures of ONFH may be beneficial for diagnosing and understanding this disease. In this work, a bone trabecula metabolomics was undertaken to determine the expression pattern of low molecular mass metabolites in patients of femoral head necrosis based on the ultra-performance liquid chromatography/time-of-flight tandem mass spectrometry (UPLC/TOF MS/MS). Histological study showed that necrotic bone was characterized by necrosis, fibrosis and lacuna, but adjacent "normal" bone was pathologically normal. Principal component analysis in combination with orthogonal partial least-squares discrimination analysis was used to find out changed metabolites. MS/MS was used to speculate the corresponding molecule. Both osteonecrotic bone trabecula (ONBT) and adjacent "normal" bone trabecula (ANBT) showed higher levels of amino acids, such as proline, arginine, glutamine, dipeptides and lower levels of antioxidants. Most disrupted lipids, such as fatty acid esters, glycerophospholipids, sphingolipids, were found in osteonecrotic zone. The area under the receiver operating characteristic curve of combinational biomarkers (D-arginine, L-proline, L-carnitine, inosine) in ONBT and ANBT was 0.996 and 0.950, respectively. Our findings might provide a significant insight to understand the metabolic mechanism and diagnosis biomarkers of ONFH in the future.

**Keywords** Metabolomics · UPLC–MS/MS · Osteonecrosis of the femoral head · Biomarkers

The authors Weiwen Zhu and Tingmei Chen have contributed equally to this work.

✉ Jian Zhang
zhangjiancqmu@sohu.com

[1] Department of Orthopedics, The First Affiliated Hospital of Chongqing Medical University, Chongqing 400016, China

[2] Key Laboratory of Clinical Laboratory Diagnostics (Ministry of Education), College of Laboratory Medicine, Chongqing Medical University, Chongqing 400016, China

## 1 Introduction

Osteonecrosis of the femoral head (ONFH) remains a major cause of total hip arthroplasty and represents a serious clinical and financial problem because it is a single great cause of attrition in the young disability (Wu et al. 2008; Shih et al. 2009). In 2014, there were approximately 7 million people with ONFH in China, and nearly 20,000 new cases were diagnosed annually in the United States (Chen et al. 2015a, b; Gangji et al. 2011). Because ONFH is considered irreversible in end stage, it is best to perform diagnostic or therapeutic strategies for ONFH in the early stage (Wen et al. 2008). Unfortunately, the early diagnosis and treatment for this disease have not been established (Chen et al. 2015a, b). ONFH is always associated with numerous risk factors, such as trauma, excessive corticosteroid administration, corticosteroid treatment, sickle cell disease, coagulopathies, autoimmune diseases and other factors. And, it is supported that ONFH might be a systemic disease (Hernigou et al. 2015; Seamon et al. 2012;

Lee et al. 2009; Asano et al. 2003). The histopathological change of ONFH is bone marrow structure disturbance, marrow cell necrosis fibrosis invasion, empty lacunae appearance in trabecula (Kang et al. 2015; Qiang et al. 2015; Ragab et al. 2008). Recent studies suggested that influenced lipid metabolism, like ApoA5, ApoA6, and high-density lipoprotein cholesterol, low-density lipoprotein cholesterol, plays a role in the process of ONFH (Gangji et al. 2011; Cui et al. 2014; Qi and Zeng 2015; Yin et al. Yin et al. 2014). The mechanism of ONFH is closely related with bone metabolism abnormality. In addition, complicated bone metabolism is altered not only in osteonecrosis zone but also in the adjacent zone of the femoral head, probably (Tingart et al. 2009; Calder et al. 2001). So far, underlying mechanisms regulating bone metabolism and remodeling in patients with ONFH still remains unknown, and no metabolite biomarkers in ONFH bone trabecula were confirmed in previous researches. As a consequence, a new approach to understand ONFH is urgently needed to get more insight into this disease.

To comprehend the relationships and interactions between genetic diversities and environmental triggers of disease, systems biology powered by genomics, proteomics, bioinformatics, and metabolomics, is providing a new logical framework to elaborate disease etiology and to excavate latent connections between seemingly disparate disease states (Holmes et al. 2008a, b). Metabolome-wide association studies are capable of linking human metabotype variations to disease risk factors in the general population (Holmes et al. 2008a, b). In addition, metabolomic analysis is furnishing answers to important questions relevant to human health and disease (Chen et al. 2011, Bjerrum et al. 2014). Metabolomics is a powerful tool to scan diagnostic biomarkers and to explore disease pathogenesis (Gertsman et al. 2014). It has been successfully applied in the study of orthopedic diseases to seek the biomarkers or metabolism mechanism, such as rheumatoid arthritis, spondyloarthritis, osteoarthritis, etc. (Priori et al. 2013; Van Wietmarschen et al. 2012; Blanco 2014). For metabolomic studies, most frequently employed high-throughout analytical methods are NMR spectroscopy and MS combined with chromatography technology such as liquid chromatography (LC) or gas chromatography (GC) (Gonzalez et al. 2012). Recently the development of ultra-performance liquid chromatography (UPLC) has made it possible to achieve higher resolutions, higher sensitivities, and rapider separations compared with LC. And UPLC combined with orthogonal acceleration time-of-flight mass spectrometry, which enables the exact mass measurements, is undoubtedly a more fitting system for metabolomics (Gonzalez et al. 2012).

To date, metabolomic technology has not been applied in the study of ONFH bone trabecula. In this work,

UPLC–MS/MS-based metabolomics was first used to determine the metabolic variation between bone of ONFH and fracture of femoral neck. We identified metabolic differences between ONFH bone tissue (ONBT and ANBT) and fracture of femoral neck bone tissue. Furthermore, we tested the efficiency of our approach for the discrimination between ONFH and femoral neck patients. The aim is to offer a new insight into the complex dysregulation of the metabolism in ONFH patients and to provide a new way for exploring potential molecular biomarkers of ONFH.

## 2 Materials and methods

### 2.1 Human samples process

This study was approved by the Ethics Committee of Chongqing Medical University and the First Affiliated Hospital of Chongqing Medical University. Written informed consents were obtained from all the subjects.

The study subjects consisted of 28 ONFH patients and 20 patients with fracture of femur (in neck or intertrochanteric zone) as controls. Patients with ONFH were recruited from the Department of Orthopedics of the First Affiliated Hospital of Chongqing Medical University between September 2014 and February 2015. Inclusion criteria: (1) ONFH identified by typical magnetic resonance imaging (MRI) and/or plain radiographs; (2) patients were in stage 3 or 4 by the Ficat classification system; (3) patients need a total hip at012hroplasty (THA) therapy. The exclusion criteria: (1) proof or history of metabolic bone diseases such as renal osteodystrophy, hyper- or hypoparathyroidism, Paget's disease, and presence of cancers with bone metastasis; (2) patients with an MRI that did not meet with diagnosis of ONFH; (3) patients who did not agree to participate in this research project. Twenty-eight patients (14 females and 14 males) were enrolled in the ONFH group. For the control group, 20 patients with fracture of femoral neck or intertrochanteric femoral (11 females and 9 males) were enrolled. Surgically resected bone tissues were obtained in the operating room from patients with ONFH (n = 28) and fracture of femoral neck or intertrochanteric femoral (tissue uninvolved by necrosis) (n = 20). A biopsy specimen was obtained to analyze the histological performance and confirm the diagnosis. The bone tissues from ONFH subjects were further divided into osteonecrotic bone trabecula (ONBT) and adjacent normal bone trabecula (ANBT) (mainly from normal junction of the femoral head and neck) according to the facade and histological examination. All specimens were stored in liquid nitrogen until analysis.

## 2.2 Medical image and histological analysis

Radiographs of the femoral head and magnetic resonance imaging (MRI) are most frequently used for the clinical diagnosis of ONFH (Fig. 1a, b). In addition, the 48 surgical specimens of all characters were paraformaldehyde -fixed, decalcified, paraffin-embedded, sectioned and stained with hematoxylin and eosin according to the standard protocols. For all the cases included in the study, histopathological review of the corresponding surgical samples was performed (Fig. 1c, d, e, f).

## 2.3 Metabolites extraction

Samples were thawed on ice. Tissue (50 mg) was homogenized in a volume of water at 200 μL in a 2-mL microtubes with two 1-mm magnetic beads, and one 5-mm beads on the high throughout tissue grinder (SCIENTZ-48, China) at 40 Hz for 5 min. The samples were extracted by a series of following solvent extraction steps: 400 μL tridecanoic acid (2.5 mg/mL) (Sigma) in ethyl acetate:

ethyl alcohol (1:1); 200 μL methanol; 200 μL methanol: $H_2O$ (3:1); and dichloromethane: methanol (1:1). Each extraction step was conducted by shaking 2 min with the magnetic beads using the tissue grinder. The samples were centrifuged and the supernatants were removed after the each extraction step, followed by re-extraction. Next, the multiple supernatants were mixed by pipetting up and down several times and a 1 mL aliquot of each sample was transferred to one 1.5-mL microtube. The samples were placed in the MTN-2800D concentrator for drying. Samples were kept on ice throughout the whole extraction process.

## 2.4 UPLC–MS/MS analysis

For UPLC–MS/MS analysis, each sample was reconstituted by an 80-μL volume of methanol with 20-μL $H_2O$ and centrifuged at 12000 g for 10 min. A 60-μL aliquot of each supernatant was transferred to the auto-sampler vial. An aliquot of 10-μL volume of each rest supernatant was pooled as QC (quality control) group.
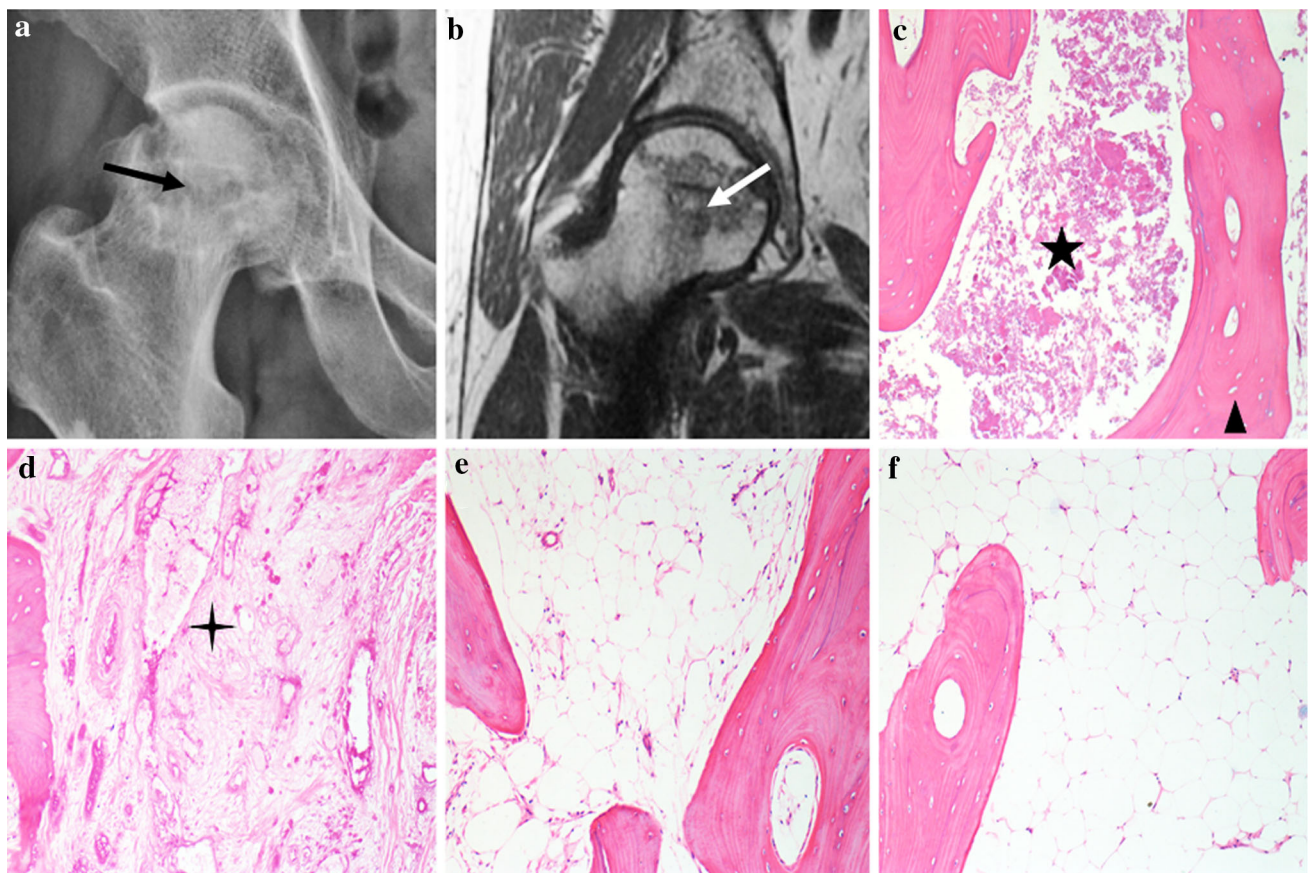


**Fig. 1** Radiograph, MRI and histological image of samples. **a**, **b** are the radiograph and MRI image of the ONFH patients. The histological performance of ONBT (**c**, **d**), ANBT (**e**) and controls (**f**) are shown in above figures. The *black* and *white arrows* show collapse of the head and subchondral bone fracture. *Triangle* shows empty lacunae in bone trabecula. *Pentagram* shows necrotic mesenchyme tissue. *Cross-star* shows dense fibrosis in canals. No obvious alteration can be seen in **e** and **f**

UPLC-Q-TOF–MS/MS analyses were conducted using a Shimadzu UFLC-equipped AB-Sciex Triple TOF 4600 in both positive and negative ionization mode using the Turbo V ESI ion source. The Triple TOF samples were injected onto an Kinetex XB-C18 column (100 mm × 2.1 mm, 2.6 μm, Phenomenex) with a flow rate of 0.35 mL/min. The mobile phase consisted of 0.1 % formic acid in water (A) and 0.1 % formic acid in acetonitrile (B). The gradient was as follows: Solvent B was held constant at 1 % for 1 min and solvent B was increased from 5 to 85 % over 8 min, following holding constant in solvent B to 85 % by 12 min and then to 5 % by 12.1 min, all the method stopped at 15 min. The nebulizer gas (air) and turbo gas (air) were set to 55 psi, respectively, the heater temperature was 600 °C. The ion spray voltage was set to 5500 V for positive ion and −4500 V for negative ion mode, respectively. The curtain gas (nitrogen) was set at 25 psi, and the rolling collision energy (CE) was set at $40 \pm 15$ V for positive ion mode and $-(40 \pm 15)$ V for negative ion mode. Full scan analysis was performed in the electrospray ionization mass spectrometry mode using electrospray ionization technique with coverage of mass range 50–1000 Da by using scan rate of 0.25 s, and the MS/MS screening was accomplished in the combinational mode of positive-information dependent acquisition (IDA) with a scan rate of 0.1 s. A 5 μL aliquot of each sample was injected onto the column. Before the samples were analysed, 10 QCs were injected for adjust the system consistency, and one QC was used to estimated system reproducibility and one blank was used to flush the column after each 5 samples were analysed.

## 2.5 Data collection and pretreatment

All the ion features were extracted, pretreated and normalized using Shortcut to MarkerView 1.2.1 and exported to text file for further analysis. The "80 % rule" (Bijlsma et al. 2006) was applied to remove the missing values. The multivariate statistical analysis was performed by the SIMCA-P software (version 13.0; Umetrics, Umea, Sweden). After the Pareto scaling (scaled to square root of variance and centralization), intrinsic clusters and outliers within the Pareto-scaled data sets were detected by principal component analysis (PCA). The orthogonal partial least-squares discrimination analysis (OPLS-DA) was applied to the data for discriminating the specimens according to different sample groups. The sevenfold cross-validation was performed to validate models.

## 2.6 Data analysis

The feature ions which can separate ONBT from controls and distinguish ANBT from ONBT are selected via the variable importance in projection (VIP) values of OPLS-DA model and p values of univariate statistic analysis. Then these feature ions are identified and assigned to corresponding metabolites. Variables, with a VIP value larger than 1, show a higher force than average on the classification. Those variables were eventually selected as potential biomarkers. The univariate test was performed on measurement data, and $p < 0.05$ was considered statistically significant. The $R^2Y(cum)$ is used to evaluate the perfection of fit of the model that indicates the fraction of explained Y-variation, and Q2(cum) suggests the ability of prediction. To confirm the potential biomarkers, their mass spectra and chromatographic retention times were compared with the available reference standards. The Shortcut to PeakView was used to facilitate the MS/MS fragment ion analysis process by way of chemically intelligent peak-matching algorithms. Then, the information was presented for database searching, either in-house or using Mass Bank (http://www.massbank.jp/) and the HMDB (http://www.hmdb.ca/). The receiver operating characteristic (ROC) curve was employed to evaluate the clinical diagnostic performance of all changed metabolites and the combination of selected metabolites. All the clinical data and metabolomics data analysis were conducted using SPSS17.0 version software. The interaction, construction, and pathway analysis of potential biomarkers was conducted with MetPA (http://metpa.metabolomics.ca./MetPA/faces/Home.jsp) via database source including the Human Metabolome Database (http://www.hmdb.ca/), SMPD (http://www.smpdb.ca/), KEGG (http://www.genome.jp/kegg/), and METLIN (http://metlin.scripps.edu/) for confirming the impacted metabolic pathways and visualization.

## 3 Results

### 3.1 Demographics and clinical characteristics

The demographics and clinical characteristics of ONFH and control subjects were depicted in Table S1. No significant difference can be seen in age, height, weight and BMI between control group and ONFH group. In ONFH group, 13 ONFH patients had a history of alcohol consumption and corticosteroid treatment, respectively. Seven ONFH patients had the history of Legg-Calve Perthes disease in childhood. Two ONFH patients had the history of trauma. In the rest six patients, no clear causes were determined. According to the Ficat classification system, all ONFH patients were staged in III or IV. Total hip arthroplasty was performed in both ONFH group and control group.

## 3.2 Medicine image of subjects and histological analysis of the samples

The results of the typical MRI or X-ray images were matched with the ONFH biopsy report (gold standard). Figure 1 displayed microscopic images of hematoxylin- and eosin-stained sections of ONFH bone tissue used for histological examination, as well as, radiograph and MRI of hip for clinical examination. In Fig. 1a, a radiograph obtained from the participants showed collapse of the head, and in Fig. 1b, T2-weighted MRI image showed the typical subchondral fracture as a band of low signal intensity. In ONBT group, Fig. 1c showed the microscopic image $(4 \times)$ of dense fibrosis in canals resulting from the repairment with disappearing of mesenchymal tissue and empty lacunae in trabecula, and a lot of avascular necrotic mesenchyme tissue and hypertrophic trabeculas (Fig. 1d). In control and ANBT tissues, normal bone tissue feature and cells were manifested in Fig. 1e, f.

## 3.3 Bone metabolite profiles of ONFH and control group based on UPLC–MS/MS

Totally 76 bone tissues (20 control, 28 ONBT, 28 ANBT) of the femoral head were analyzed with RPLC (Reversed Phase Liquid Chromatography)-MS/MS and HILIC (Hydrophilic interaction chromatography)-MS/MS in both positive ion mode and negative ion mode. Fifteen QC samples were run (one QC after each 5 samples, five QC before each 20 samples to adjust the stability of the machine). After aligning peaks, Pareto scaling, normalization, and removing the zero-values by the 80 % rule, eventually 67 metabolites within measurement errors (<10 ppm), were annotated from the spectral features from UPLC–MS/MS using reference standards as well as the available database (HMDB, Massbank). Several metabolites were confirmed by standards.

The reproducibility of analysis may be affected by source contamination or the maintenance and cleaning of the mass spectrometer in large-scale non-targeted LC–MS/MS metabolomics measurements. The reproducibility of metabolomics analysis was assessed by QC samples. The PCA score plots of normalized positive ion mode data set was shown in Fig. S1. It can be seen that QC samples were tightly clustered together in the middle zone. This result demonstrates that the reproducibility is favorable. Furthermore, the reproducibility of the ions was evaluated by relative standard deviation (RSD %) of 8 randomly picked peak in the 10 QC samples. In RPLC-POS, HILIC-POS, RPLC-NEG, HILIC-NEG modes, the fluctuation range of RSD % was 5.3–12.7, 0.7–5.3, 2.2–10.2 and 1.1–4.2 %, respectively. The results give rise to that the reproducibility

of our platform was excellent for the metabolomic profile study.

## 3.4 Multivariate analysis

To distinguish ONBTs and ANBTs from the controls, PCA and orthogonal partial least squares-discriminant analysis (OPLS-DA) were employed (Fig. S2). There is a separation between controls and ONFH subjects (including ONBT and ANBT groups), reflecting the pathophysiological variations of ONFH. Notably, in PCA and OPLS-DA recognition models, the metabolic patterns of ONBT and ANBT were separated from that of the controls. However, in PCA model, clear distinction can hardly be seen among the metabolite profiles of the ONBTs and ANBTs, and in OPLS-DA model, tight adjacence can be seen between ONBTs and ANBTs. Partly-similar variety were shown in metabolism between the ONBTs and ANBTs (Fig. S2).

## 3.5 Metabolite profiles of ONBT, ANBT and control specimens

Based on VIP value (>1) in OPLS-DA analysis ($Q^2 > 0.5$, $R^2X > 0.5$, $R^2Y > 0.5$) (Fig. 2) and Mann–Whitney U test p value(<0.05), 52 metabolites were significantly altered in ONBT samples compared to the controls. These metabolites were further identified following recently published strategy (Gonzalez et al. 2012). Accurate mass and mass spectrometric fragmentation patterns of the changed metabolites were utilized to search databases including KEGG, Massbank, METLIN, and HMDB. In addition, some amino acids were validated by running available standards. The results were summarized in Table 1. These metabolites participate in key metabolic pathways, like amino acid metabolism, lipid metabolism, nucleotide metabolism and pyrrolidines metabolism. For the metabolite profiles of ANBT and control samples (Fig. 3), 20 differentiated metabolites in ONBT also showed significant distinctiveness in ANBT group, like uracil, L-carnitine, L-valine, D-arginine, L-proline, L-tyrosine, phylloquinone, hypoxanthine, etc. (Table 1). However, there are still 16 changed metabolites in ANBT, such as, guanine, narceine, DG, germanicol cinnamate, beta-D-galactose, etc.

## 3.6 Metabolism pathway analysis

By the analysis of MetPA (Fig. S3a), these metabolism pathway may be considered as the critical points, including D-Arginine and D-ornithine metabolism, D-Glutamine and D-gultamate metabolism, proline, valine, leucine and isoleucine metabolism. Results of MetPA (Fig. S3b) implied that although no histopathological altering, metabolism in
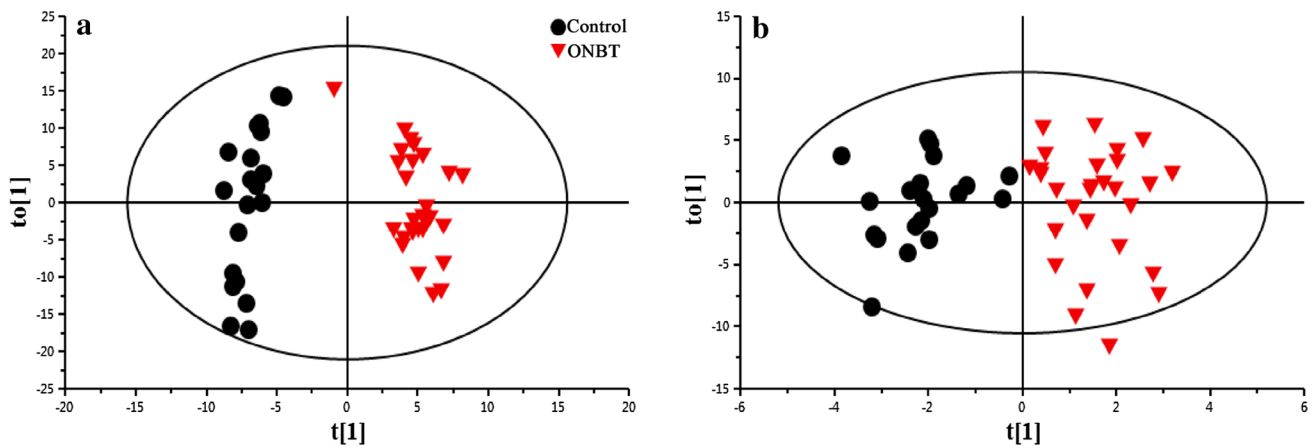
**Fig. 2** OPLS-DA scores plot of control and ONBT groups in ESI positive (**a**) and ESI negative models (**b**). In **a** $R^2X$ (cum) $= 0.526$, $R^2Y$ (cum) $= 0.944$, $Q^2$ (cum) $= 0.796$. In **b** $R^2X$ (cum) $= 0.696$, $R^2Y$ (cum) $= 0.820$, $Q^2$ (cum) $= 0.601$

adjacent zone show apparent distinction in D-arginine and D-ornithine metabolism, D-glutamine and D-gultamate metabolism, pyrimidine and purine metabolism, alamine, proline, valine, leucine and isoleucine metabolism. It can be detected that a large part of the metabolism pathways in ANBT were the same as that between ONBT and control groups.

### 3.7 Validation of the metabolic biomarker

All the 67 differentiated metabolites were summarized in Table 1. The variation trend of metabolites in controls, ANBTs and ONBTs were shown in the heatmap (Fig. 4). Compared with the controls, 45 metabolites increased and 22 metabolites decreased in ONFH (ANBTs or ONBTs) subjects. The increased metabolites in ANBT group also increased more obviously in ONBT group, which suggested that ANBT might be intermediate tissue between normal and necrosis. The metabolites with AUC (area under the curve of ROC) >0.85, VIP value >2 and fold change >3 in ANBT and ONBT were picked out as potential biomarkers. The methods were described in Sect. 3.5. So, after binary logistic regression analysis, the 4 above mentioned discrepant metabolites were analyzed using receiver operating characteristic (ROC) curve to estimate sensitivity and specificity of the potential biomarkers. The AUC (area under the curve) of combined biomarkers in ONBT and ANBT were 0.989 and 0.928 and the ROC curves of combined biomarkers were shown in Fig. 5. To validate diagnosis capability of the combinational biomarker of ONFH, another batch of samples were collected including 8 controls, 8 ONBTs, 8 ANBTs. The metabolites were measured using UPLC–MS/MS with the same criterion as depicted in contents above. The results were similar with that in the previous discovery phase

samples by PCA and OPLS-DA analysis, and the AUC of the combinational biomarker are 0.900 and 0.990 in ANBT and ONBT groups (Fig. S4).

## 4 Discussion

In the present study, we applied a metabolomics approach to determine the metabolic distinction between ONFH and control subjects and understand how those metabolic profiles were affected by this disease. Metabolomic technology has been indicated as a powerful methods for the identification and relative quantities of metabolites, which changed resulted from disease or therapeutic intervention (Sreekumar et al. 2009). The OPLS-DA analysis of the controls and ONFH (including ONBT and ANBT samples) subjects revealed that both the tissues from ONBT and ANBT had a clearly distinct metabolic profile from controls. The partial similarity of varied metabolites in adjacent normal bone traubecula and necrotic traubecula may be suggestive of that adjacent normal traubecula is in early stage of ONFH. The analysis of MetPA indicated that the pathways of D-arginine and D-ornithine metabolism (impact value 0.32 and 0.323), arginine and proline metabolism (impact value 0.134 and 0.102) and D-glutamine, D-gutamate metabolism (impact value 0.123), alanine, aspartate, glutamate metabolism (impact value 0.207) in ONBT and ANBT were disturbed, respectively.

In total, 52 metabolites in ONBT and 35 in ANBT were identified, including prenol lipids, fatty acid esters, alkylamines, glycerolipids, peptides, amino acids and derivatives. These results were consistent with popular concepts of ONFH, including disregulated lipid metabolism and extensive disordered osteocytes metabolism beyond the necrosis zone (Tingart et al. 2009, Calder et al. 2001).

Table 1 List of differential metabolites in ONBT and ANBT samples relative to the controls

| Metabolites | rt (min) | Error (ppm) | Trend and change fold | Accurate mass | Formula | Class | Metabolism pathway | In ONBT or ANBT group | p |
|---|---|---|---|---|---|---|---|---|---|
| L-Isoleucine[a] | 5.12 | 0.3 | ↑10.2° | 131.0946 | C6H13NO2 | Amino acids | Valine, leucine and isoleucine metabolism | O | 0.003° |
| Creatine | 7.65 | −1.2 | ↑3.0° | 131.0694 | C4H9 N3O2 | Amino acids | Arginine and proline metabolism | O | 0.000° |
| L-Proline[a] | 7.46 | −1.5 | ↑4.7° ↑3.2[a] | 115.0633 | C5H9 NO2 | Amino acids | Arginine and proline metabolism | O, A | 0.000° 0.020[a] |
| D-Arginine | 5.61 | 0.3 | ↑18.0° ↑14.0[a] | 174.1116 | C6H14N4O2 | Amino acids | D-arginine and D-ornithine metabolism | O, A | 0.000° 0.000[a] |
| L-Glutamine[a] | 7.93 | −1.7 | ↑9.5° ↑4.3[a] | 146.0691 | C5H10N2O3 | Amino acids | Glutamate metabolism | O, A | 0.000° 0.021[a] |
| L-Leucine[a] | 6.81 | −1.8 | ↑3.6° ↑3.2[a] | 131.0946 | C6H13NO2 | Amino acids | Leucine metabolism | O, A | 0.000° 0.003[a] |
| L-Tyrosine[a] | 7.25 | −1.3 | ↑3.7° ↑3.4[a] | 181.0738 | C9H11NO3 | Amino acids | Phenylalanine and tyrosine metabolism | O, A | 0.000° 0.000[a] |
| L-Valine[a] | 7.13 | −2.3 | ↑3.6° ↑2.4[a] | 117.0789 | C5H11NO2 | Amino acids | Valine, leucine and isoleucine degradation | O, A | 0.000° 0.000[a] |
| L-4-hydroxyglutamate semialdehyde | 0.63 | −2.4 | ↑3.4° | 147.0531 | C5H9NO4 | Amino acids derivatives | Arginine and proline metabolism | O | 0.012° |
| Neurine | 1.06 | 0.8 | ↑1.7° | 103.0997 | C5H13NO | Alkaloids and derivatives | – | O | 0.000° |
| Uric acid | 11.42 | −0.1 | ↑5.0° ↑3.0[a] | 168.0283 | C5H4N4O3 | Alkaloids and derivatives | Purine metabolism | O,A | 0.000° 0.015[a] |
| 1-(beta-D-glucopyranosyloxy)-3-octanone | 8.65 | 3.3 | ↑2.7° | 306.1678 | C14H26O7 | Alkyl glycosides | – | O | 0.000° |
| 3-Aminopropionaldehyde | 10.59 | 99 | ↓1.7° ↑3.0[a] | 73.0527 | C3H7NO | Alkylamines | Beta-alanine metabolism | O, A | 0.000° 0.000[a] |
| Ureidoisobutyric acid | 7.93 | −1.7 | ↑7.6[a] | 146.0691 | C5H10N2O3 | Alkylamines | Pyrimidine metabolism | A | 0.000[a] |
| Benzyl glycinate | 5.02 | 0.6 | ↑15.0° | 165.0789 | C9H11NO2 | Alpha amino acid esters | AMINO acid metabolism | O | 0.000° |
| N-Acetylmuramoyl-ala | 6.4 | 0.9 | ↓1.8° ↑1.8[a] | 364.1481 | C14H24N2O9 | Aminosaccharides | – | O, A | 0.002° 0.000[a] |
| Terephthalic acid | 1.38 | −0.8 | ↑2.2[a] | 166.0266 | C8H6O4 | Benzoic acid | – | A | 0.003[a] |
| Monoethylhexyl phthalic acid | 1.43 | −0.5 | ↑2.6° | 278.1518 | C16H22O4 | Benzoic acid and Derivatives | – | O | 0.000° |
| Uracil | 5.74 | −0.6 | ↑50° ↑40[a] | 112.0272 | C4H4N2O2 | Diazines | Beta-alanine metabolism and pyrimidine metabolism | O, A | 0.000° 0.000[a] |

**Table 1** continued

| Metabolites | rt (min) | Error (ppm) | Trend and change fold | Accurate mass | Formula | Class | Metabolism pathway | In ONBT or ANBT group | p |
|---|---|---|---|---|---|---|---|---|---|
| Vitamin K (phylloquinone) | 8.37 | 0.6 | ↓2.6°/↑1.5ᵃ | 450.3497 | C31H46O2 | Diterpenes | Vitamin metabolism. | O, A | 0.000°/0.000ᵃ |
| 2,3-Diacetoxypropyl stearate | 8.87 | 0.5 | ↑1.5ᵃ | 442.3294 | C25H46O6 | Fatty acid esters | Lipid metabolism | A | 0.000ᵃ |
| Butyrylcarnitine | 5.82 | 0.1 | ↑3.6ᵃ | 231.1470 | C11H21NO4 | Fatty acid esters | Lipid metabolism | O | 0.005ᵃ |
| Diethylhexyl adipate | 1.34 | −2.9 | ↑1.8ᵃ | 370.3083 | C22H42O4 | Fatty acid esters | Lipid metabolism | O | 0.002ᵃ |
| L-Acetylcarnitine | 6.45 | −0.3 | ↑3.1° | 203.1157 | C9H17NO4 | Fatty acid esters | Fatty acid beta-oxidation | O | 0.002° |
| Sorbitan oleate | 8.52 | −1.7 | ↓1.4°/↑1.5ᵃ | 428.3137 | C24H44O6 | Fatty acid esters | Pentoses | O, A | 0.000°/0.000ᵃ |
| DHAP(18:0) | 5.63 | 0.6 | ↑2.1ᵃ | 436.2589 | C21H41O7P | Fatty acid esters | Plasmalogen synthesis | A | 0.039ᵃ |
| (2′E,4′Z,7′Z,8E)-colnelenic acid | 1.58 | 1.6 | ↓1.4°/↑1.8ᵃ | 292.2038 | C18H28O3 | Fatty acids | Alpha-Linolenic acid metabolism | O, A | 0.012°/0.002ᵃ |
| 2-Oxo-4-methylthiobutanoic acid | 1.43 | 0.3 | ↑2.5° | 148.0194 | C5H8O3S | Fatty acids | Methionine metabolism | O | 0.000° |
| 1,3-Diacetoxy-4,6,12-tetradecatriene-8,10-diyne | 1.42 | 0.5 | ↑2.7° | 300.1361 | C18H20O4 | Fatty alcohol esters | Lipid metabolism | O | 0.000° |
| L-Carnitine | 6.89 | −0.7 | ↑6.3°/↑3.6ᵃ | 161.1051 | C7H15NO3 | Fatty acyls | Beta-oxidation of fatty acids | O, A | 0.000°/0.000ᵃ |
| PC(18:1(9Z)/14:0) | 8.2 | 0.9 | ↓1.6° | 731.5465 | C40H78NO8P | Glycerophospholipids | Glycerophospholipid metabolism | O | 0.000° |
| LysopE(18:0/0:0) | 7.76 | 0.2 | ↑12.78ᵃ | 481.3168 | C23H48NO7P | Glycerophospholipids | Glycerophospholipids | A | 0.000ᵃ |
| PE(14:1(9Z)/p-18:1(9Z)) | 8.24 | −0.3 | ↓1.6ᵃ | 671.4889 | C37H70NO7P | Glycerophospholipids | Glycerophospholipids metabolism | A | 0.000ᵃ |
| LysoPC(14:0) | 5.62 | 0.5 | ↑2.8° | 467.3011 | C22H46NO7P | Glycerophospholipids | Lipid metabolism | O | 0.001° |
| LysoPC(16:0) | 5.57 | 0.2 | ↑1.7° | 495.3324 | C24H50NO7P | Glycerophospholipids | Lipid metabolism | O | 0.011° |
| LysoPC(20:4(5Z,8Z,11Z,14Z)) | 5.53 | 2.5 | ↑2.36° | 543.3324 | C28H50NO7P | Glycerophospholipids | Lipid metabolism | O | 0.001° |
| LysoPE(22:6(4Z,7Z,10Z,13Z,16Z,19Z)/0:0) | 4.5 | 0.5 | ↓1.55° | 525.2855 | C27H44NO7P | Glycerophospholipids | Lipid metabolism | O | 0.000° |
| PC(20:1(11Z)/18:3(6Z,9Z,12Z)) | 5.41 | 1.6 | ↑2.5° | 809.5934 | C46H84NO8P | Glycerophospholipids | Lipid metabolism | O | 0.001° |
| PC(22:4(7Z,10Z,13Z,16Z)/14:0) | 5.43 | −2.5 | ↑1.7° | 781.5621 | C44H80NO8P | Glycerophospholipids | Lipid metabolism | O | 0.003° |
| PE(P-16:0e/0:0) | 7.57 | 0.2 | ↑8.5° | 437.2906 | C21H44NO6P | Glycerophospholipids | Lipid metabolism | O | 0.001° |
| 5,6-Dihydroxyindole | 7.05 | −0.7 | ↑6.0° | 149.0476 | C8H7NO2 | Hydroxyindoles | Tyrosine metabolism | O | 0.000° |
| Guanine | 6.38 | 1.1 | ↑10.1ᵃ | 151.0494 | C5H5N5O | Imidazopyrimidines | Purine metabolism | A | 0.000ᵃ |
| Hypoxanthine | 5.78 | −5.2 | ↑3.8°/↑2.3ᵃ | 136.0385 | C5H4N4O | Imidazopyrimidines | Purine metabolism | O, A | 0.039°/0.015ᵃ |
| (R)-pronuciferine | 8.6 | 3.5 | ↓2.63° | 311.1521 | C19H21NO3 | Isoquinolines | – | O | 0.000° |
| Beta-D-galactose | 6.95 | 1.1 | ↑6.5ᵃ | 180.0633 | C6H12O6 | Monosaccharides | Galactose metabolism | A | 0.000ᵃ |

**Table 1** continued

| Metabolites | rt (min) | Error (ppm) | Trend and change fold | Accurate mass | Formula | Class | Metabolism pathway | In ONBT or ANBT group | p |
|---|---|---|---|---|---|---|---|---|---|
| Asparaginyl-proline | 7.01 | −1.1 | ↑2.9ᵃ | 229.1062 | C9H15N3O4 | Peptides | Amino acids metabolism | A | 0.006ᵃ |
| Alanyl-aspartate | 1.43 | 0.2 | ↑2.3° | 204.0746 | C7H12N2O5 | Peptides | Amino acids metabolism | O | 0.000° |
| Histidinyl-lysine | 8.85 | 3.9 | ↓2.0° | 283.1644 | C12H21N5O3 | Peptides | Amino acids metabolism | O | 0.000° |
| L-Prolyl-L-phenylalanine | 1.42 | −0.3 | ↑8.8° ↑4.2ᵃ | 262.1317 | C14H18N2O3 | Peptides | Amino acids metabolism | O, A | 0.000° 0.000ᵃ |
| Phenylalanyl-methionine | 6.4 | 2.4 | ↓1.7° ↓1.6ᵃ | 296.1194 | C14H20N2O3S | Peptides | Amino acids metabolism | O, A | 0.000° 0.000ᵃ |
| Citranaxanthin | 9.31 | −0.3 | ↓1.5ᵃ | 456.3392 | C33H44O | Prenol lipids | Lipid metabolism | A | 0.000ᵃ |
| Germanicol cinnamate | 8.32 | 1.2 | ↓1.55ᵃ | 556.4280 | C39H56O2 | Prenol Lipids | Lipid metabolism | A | 0.000ᵃ |
| Pisumionoside | 7.93 | 0.9 | ↑5.1ᵃ | 404.2046 | C19H32O9 | Prenol lipids | Lipid metabolism | A | 0.000ᵃ |
| Rubixanthin | 8.76 | 1 | ↓1.5ᵃ | 552.4331 | C40H56O | Prenol lipids | Lipid metabolism | A | 0.000ᵃ |
| (4S,8R)-8,9-dihydroxy-p-menth-1(6)-en-2-one | 1.73 | 0.5 | ↑2.2° | 184.1099 | C10H16O3 | Prenol lipids | Lipid metabolism | O | 0.001° |
| 3-Methyl-2-butene-1-thiol | 6.67 | −3 | ↑3.1° | 102.0503 | C5H10S | Prenol lipids | Lipid metabolism | O | 0.001° |
| Beta-cryptoxanthin | 8.76 | 1 | ↓1.6° | 552.4331 | C40H56O | Prenol lipids | Lipid metabolism | O | 0.000° |
| 3,6-Epoxy-5,5',6,6'-tetrahydro-b,b-carotene-3',5,5',6'-tetrol | 8.74 | −0.4 | ↓1.4° ↑1.4ᵃ | 618.4284 | C40H58O5 | Prenol lipids | Lipid metabolism | O, A | 0.000° 0.000ᵃ |
| Deterrol stearate | 9.29 | 0.6 | ↓1.6ᵃ | 478.3810 | C33H50O2 | Prenol lipids | Lipid metabolism | A | 0.000ᵃ |
| Inosine | 6.25 | 0 | ↑9.1° ↑3.7ᵃ | 268.0807 | C10H12N4O5 | Purine nucleosides | Purine metabolism | O,A | 0.000° 0.023ᵃ |
| Uridine | 3.18 | 0.8 | ↑4.0° | 244.0695 | C9H12N2O6 | Pyrimidine nucleosides | Pyrimidine metabolism | O | 0.000ᵃ |
| Pyrrolidonecarboxylic acid | 7.93 | −1.3 | ↑7.8° ↑5.6ᵃ | 129.0425 | C5H7NO3 | Pyrrolidines | D-glutamine and D-glutamate metabolism | O, A | 0.000° 0.014ᵃ |
| Pyrrolidine | 7.33 | −8.8 | ↑1.9° ↑6.64ᵃ | 71.0734 | C4H9N | Pyrrolidines | Ornithine metabolism | O, A | 0.000° 0.015ᵃ |
| AS 1-1 | 8.67 | −0.6 | ↓1.5° | 685.5128 | C38H71NO9 | Sphingolipids | Sphingolipids metabolism | O | 0.000° |
| 2-Methoxyestrone | 8.59 | 0.3 | ↓2.6° | 300.1725 | C19H24O3 | Steroid derivatives | Steroid hormone biosynthesis | O | 0.000° |
| Narceine | 3.36 | −1 | ↑5ᵃ | 445.1736 | C23H27NO8 | stilbenes | – | A | 0.000ᵃ |
| Norsalsolinol | 0.95 | −0.8 | ↑2.3 | 165.0789 | C9H11NO2 | Tetrahydroisoquinolines | – | O | 0.021° |

"rt" represents retention time. Arrows show increase or decrease in the ONBT/ANBT compared with that in controls. In first column, [a] is validated with standard samples. In fourth and the last column, [a] is found in ANBT and [o] is found in ONBT. In ninth column, "O" suggests changed metabolites were found in ONBT, "A" suggests changed metabolites were found in ANBT, "A, O" suggests changed metabolites were found both in ANBT and ONBT. "p" represents p value of univariate statististics
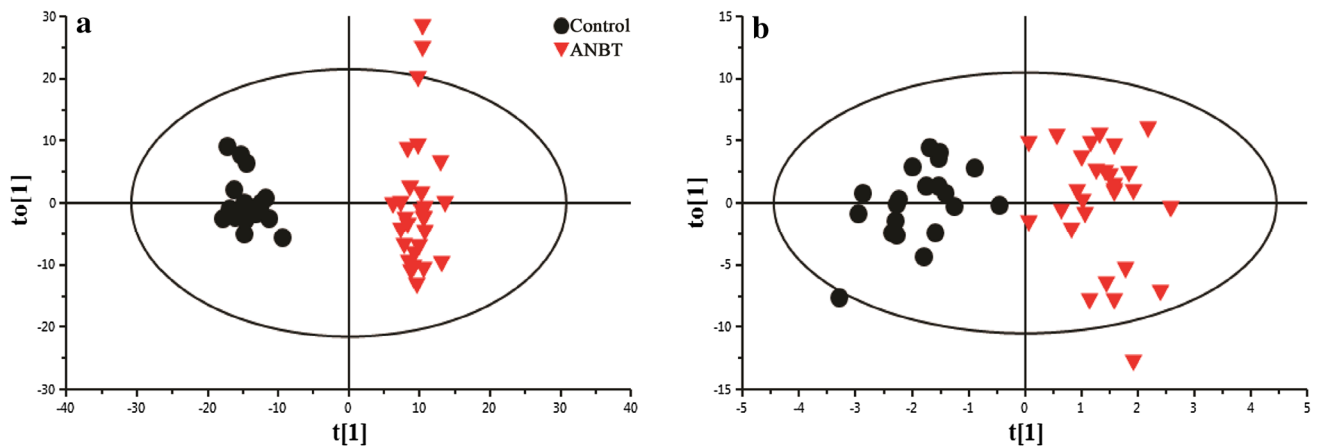
**Fig. 3** OPLS-DA scores plot of control and ANBT groups in ESI positive (**a**) and ESI negative models (**b**). In **a** $R^2X$ (cum) = 0.792, $R^2Y$ (cum) = 0.976, $Q^2$ (cum) = 0.879. In **b** $R^2X$ (cum) = 0.642, $R^2Y$ (cum) = 0.866, $Q^2$ (cum) = 0.705



**Fig. 4** Heat map of differential metabolites corresponding to Table 1
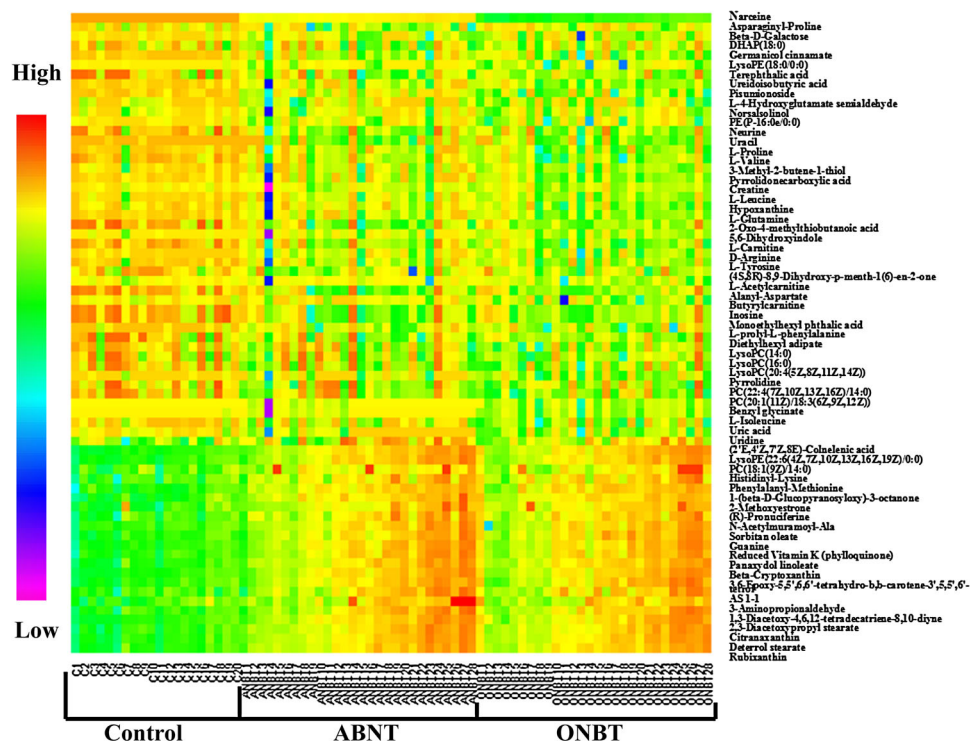
Glycerophospholipids occupied a large part of the distinctive metabolites between ONBT and the controls, like LysoPC (16:0), PC (22:4(7Z,10Z,13Z,16Z)/14:0), LysoPC (20:4(5Z,8Z,11Z,14Z)), PC(20:1(11Z)/18:3(6Z,9Z,12Z)), LysoPC (14:0), PE(P-16:0e/0:0), LysoPE (22:6(4Z,7Z,10Z, 13Z,16Z,19Z)/0:0), PC(18:1(9Z)/14:0). Most of them are up-regulated in ONFH characters. The study presented by Braverman et al. suggested that glycerophospholipids might protect against ischemic damage and have additional functions in cardiac sarcolemma (Braverman and Moser 2012). Fukumoto et al. inferred that glycosyltransferase

inhibitor D-PDMP inhibited osteclastogenesis and the RANKL-induced phosphorylation of Akt, located downstream of RANK, and disruption of lipid rafts influenced actin ring formation and lead to apoptosis in osteoclasts. So glycosphingolipids are important for the RANKL-induced osteoclastogenesis via lipid rafts (Fukumoto et al. 2006). Defects in the biosynthesis of plasmalogens, the most abundant form of alkenyl-glycerophospholipids, seems to affect the process of endochondral ossification through a delay or arrest in chondrocyte maturation (da Silva et al. 2012). Taken together, both osteoclast and osteoblast in

**Fig. 5** ROC of combined biomarkers in ANBT (**a**) and ONBT (**b**) groups. *Red curve* is the combined biomarker ROC curve. AUC in **a** is 0.928 and in **b** is 0.989 (Color figure online)
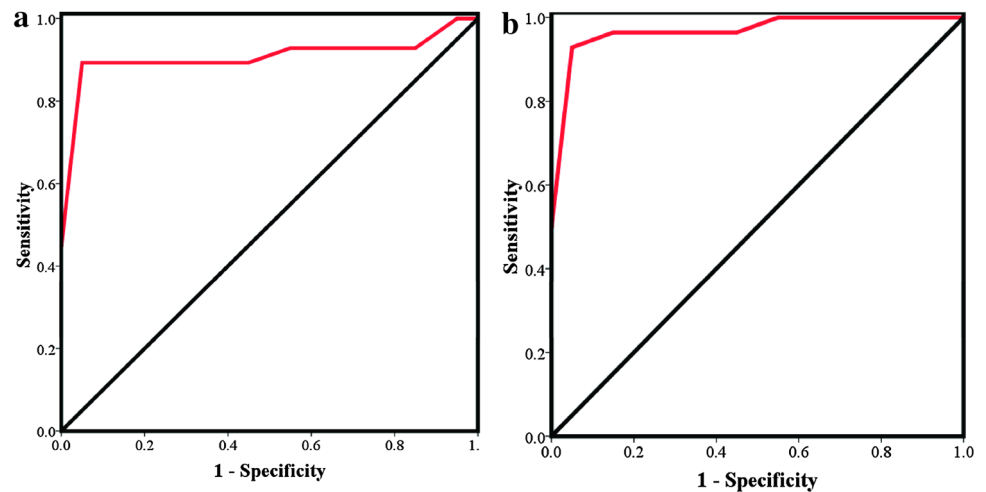


bone can be affected by glycerophospholipids. These discoveries agreed with our results of disordered glycerophospholipids metabolism, and suggest that glycerophospholipids play a vital regulation role in the pathology process in ONFH.

L-carnitine and L-acetylcarnitine, involved in the transport of acetyl-CoA into mitochondria (Jogl and Tong 2003), are the critical point of carnitine-dependent transport of long-chain fatty acids and indispensable for β-oxidation (Nada et al. 1995). Carnitine exerted a dominant effect on osteoblast differentiation and mineralization in NIH3T3 cells by the IGF-1/PI3K/Akt signaling pathway. Osteoblast proliferation is positively affected by 10 μM L-carnitine, but negatively by the higher concentration of L-carnitine (100 μM) compared with the control (Ge et al. 2015). Also, combination of L-carnitine and taurine is shown to inhibit the proliferation and osteoblastic differentiation of vascular smooth muscle cells, dose and time-dependently (Xie et al. 2010). In addition, carnitine is reported to be capable to effect bone fracture healing due to the anti-osteoporotic, anti-inflammatory, anticytokine and antioxidant properties of it (Aydin et al. 2015). According to the study of Frey JL, specification and differentiation of osteoblasts in bone and global energy homeostasis is regulated by inducing the expression of key enzymes required for fatty acid β-oxidation (Frey et al. 2015). Herein, it can be suggested that β-oxidation process might act an important part in ONFH via affecting osteoblasts function.

It is interesting that On some reductant prenol lipids were measured, such as beta-cryptoxanthin, 3,6-epoxy-5,5′,6,6′-tetrahydro-b,b-carotene-3′,5,5′,6′-tetrol, citranaxanthin and deterrol stearate. β-cryptoxanthin, citranaxanthin and reticulataxanthin are in the class of carroteniod. Among various carotenoids, β-cryptoxanthin was found to have a stimulatory effect on bone mineralization and has stimulatory effects on osteoblastic bone formation and

contrary effects on osteoclastic bone resorption (Yamaguchi 2012, Yamaguchi and Weitzmann 2009). Antioxidative carotenoids caused increment in calcium content, alkaline phosphatase activity and deoxyribonucleic acid (DNA) content in diaphyseal and metaphyseal tissues. Carotenoids are associated with improved bone health by suppressing the osteoclast formation (Tadaishi et al. 2014). In our study, the decrease of all carotenoids in ANBT and ONBT group is indicative of bone necrosis responding to the disease. Vitamine K is able to modestly elevate the bone mass of the total radius in rabbits by regulating the calcium and phosphorus metabolism(O'Connor et al. 2015). As well, reduced vitamine K is more likely to have progression of articular cartilage and bone damage (Shea et al. 2015). Consistant with previous results, vitamin k is lessened in the ONFH subjects' bone tissue, which reflects the impaired calcium and phosphorus metabolism.

A lot of amino acids and derivatives increased both in ONBT and ANBT samples, including proline, tyrosine, arginine, leucine, valine, glutamine, tyrosine, isoleucine, creatine, L-4-hydroxyglutamate, semialdehyde benzyl glycinate. It is reported that matrix metalloproteinases degrading collagen in bone are activated by nutrient stress to make proline available (Phang et al. 2010). Collagen in bone is an abundant reservoir for proline and metabolism of proline generates electrons to produce ROS and initiates a variety of downstream effects, including blockade of the cell cycle, autophagy, and apoptosis (Phang et al. 2008). Hydroxyproline, the product of proline, in serum or urine has been considered as one the biochemical indicators of bone necrosis (Shi et al. 2010). In addition, prolidase activity has been investigated in various disorders such as Legg–Calve–Perthes disease disease, osteoporosis, osteoarthritis, uremic bone disease, and osteogenesis imperfecta (Altay et al. 2011). Proline was correlated with prolidase and bone collage metabolism (Smith et al. 1979),

which might become a potentially interesting candidate biomarker of osteonecrosis. L-arginine, with the osteoprotective effects (El-Maraghy and Mehana 2015), is able to encourage cell attachment, proliferation, and differentiation in bone (Brasinika et al. Brasinika et al. 2015). The increment of L-arginine may be the result from osteoblasts compensation. It is reported that glutamine and alanine are generally involved in carbohydrate metabolism among different cell types (Sutton-McDowall et al. 2015), and glutamine catabolism, involving pyrrolidonecarboxylic acid, mediates bone anabolism (Karner et al. 2015). Experimental studies have revealed that creatine supplementation can improve bone biomechanical parameters and bone mineral density (BMD) in Sprague–Dawley rats (Antolic et al. 2007). Consistent with the results of previously mentioned study, in our work, D-arginine and D-ornithine metabolism, arginine and proline metabolism, and D-glutamine, D-gutamate metabolism pathways were inferred critical pathological metabolism involved in ONFH. More importantly, these promising amino acid and derivates biomarkers could provide guidance for clinical diagnosis and therapy of ONFH.

Several dipeptides, like asparaginyl-proline, L-prolyl-L-phenylalanine, alanyl-aspartate, were up-regulated but phenylalanyl-methionine and histidinyl-lysine were down-regulated in ONFH. As the incomplete breakdown products of protein digestion or protein catabolism, the disturbed metaholism of dipeptides may reflect the variation of RNA world (van der Gulik and Speijer 2015), and histidine containing dipeptides was reported to have protective effects of histidine-dipeptides against progression of metabolic syndrome (Song et al. 2014). Increased uric acid, hypoxanthine, guanine and inosine are involved in purine metabolism. The disordered purine metabolism causing decreased osteoclastogenesis and an intrinsic defect of osteoblast function with subsequent low bone formation (Sauer et al. 2009). Herein, purine metabolism altering was considered as a part in ONFH pathology.

Our future study will investigate the relationship between the concentration of the potential biomarkers in serum or urine with patients with ONBT early onset of disease (patients with condition having ANBT like symptoms only), and control subjects.

# 5 Conclusions

In the present experience, based on UPLC–MS/MS metabolomics approach, the metabolic changes of ONFH patients were investigated. It is noteworthy that the variations in metabolites compositions observed between ONFH and control patients could be used to suggest the involvement of metabolic pathways to the insurgence of the disease. The

identified sixty-seven potential metabolites, potential biomarkers, associated with sphingolipid metabolism, β-oxidation, D-arginine and D-ornithine metabolism, arginine and proline metabolism, and D-glutamine, D-gutamate metabolism pathways were contributed to ONFH progress. Combination of biochemistry and histopathology results suggested that ABNT may stay the interim period between normality and necrosis. Lipid metabolism is perturbed mainly in necrotic period, and disturbed amino acid metabolism was infered to occur in the whole disease process. Four metabolites including D-arginine, L-proline, L-carnitine, inosine, were picked out as potential biomarkers. A combinational biomarker of these 4 metabolites characterized by AUC >0.85, VIP value >2 and fold change >3 both in ANBT and ONBT, showed good sensitivity and specificity. More study will be investigated to excavate the complex pathological mechanisms. Further refinement and validation of these biomarkers and metabolism mechanism in larger cohorts of patients would be of considerable interest.

### Compliance with ethical standards

**Conflict of interest** The authors declare no conflict of interest.

**Human and animal rights** All procedures performed in studies involving human participants were in accordance with the ethical standards of the institutional and/or national research committee and with the 1964 Helsinki declaration and its later amendments or comparable ethical standards

**Informed consent** Informed consent was obtained from all participants for being included in the study.

# References

Altay, M. A., Erturk, C., Aksoy, N., et al. (2011). Serum prolidase activity and oxidative–antioxidative status in Legg–Calve–Perthes disease. *Journal of Pediatric Orthopaedics Part B, 20*(4), 222–226.

Antolic, A., Roy, B. D., Tarnopolsky, M. A., et al. (2007). Creatine monohydrate increases bonemineral density in young Sprague-Dawley rats. *Medicine and Science in Sports and Exercise, 39*(5), 816–820.

Asano, T., Takahashi, K. A., Fujioka, M., et al. (2003). Genetic analysis of steroid-induced osteonecrosis of the femoral head. *Journal of Orthopaedic Science: official journal of the Japanese Orthopaedic Association, 8*(3), 329–333.

Aydin, A., Halici, Z., Albayrak, A., et al. (2015). Treatment with Carnitine Enhances Bone Fracture Healing under Osteoporotic

and/or Inflammatory Conditions. *Basic & Clinical Pharmacology & Toxicology,*. doi:10.1111/bcpt.12384.

Bijlsma, S., Bobeldijk, I., Verheij, E. R., et al. (2006). Large-scale human metabolomics studies: a strategy for data (pre-) processing and validation. *Analytical Chemistry, 78*(2), 567–574.

Bjerrum, J. T., Wang, Y., Hao, F., et al. (2014). Metabonomics of human fecal extracts characterize ulcerative colitis, Crohn's disease and healthy individuals. *Metabolomics: Official Journal of the Metabolomic Society, 13*(2), 122–133.

Blanco, F. J. (2014). Osteoarthritis Year in Review 2014: we need more biochemical biomarkers in qualification phase. *Osteoarthritis and Cartilage, 22*(12), 2025–2032.

Brasinika, D., Tsigkou, O., Tsetsekou, A., & Missirlis, Y. F. (2015). Bioinspired synthesis of hydroxyapatite nanocrystals in the presence of collagen and L-arginine: Candidates for bone regeneration. *Journal of Biomedical Material Research Part B: Applied materials,*. doi:10.1002/jbm.b.33413.

Braverman, N. E., & Moser, A. B. (2012). Functions of plasmalogen lipids in health and disease. *Biochimica et Biophysica Acta-Molecular Basis of Disease, 1822*(9), 1442–1452.

Calder, J. D., Pearse, M. F., & Revell, P. A. (2001). The extent of osteocyte death in the proximal femur of patients with osteonecrosis of the femoral head. *The Journal of bone and joint Surgery, British, 83*(3), 419–422.

Chen, S. B., Hu, H., Gao, Y. S., He, H. Y., Jin, D. X., & Zhang, C. Q. (2015a). Prevalence of Clinical Anxiety, Clinical Depression and Associated Risk Factors in Chinese Young and Middle-Aged Patients with Osteonecrosis of the Femoral Head. *PLoS One, 10*(3), e0120234.

Chen, Y., Zeng, C., Zeng, H., et al. (2015b). Comparative serum proteome expression of the steroid-induced femoral head osteonecrosis in adults. *Experimental and Therapeutic Medicine, 9*(1), 77–83.

Chen, J., Zhang, X., Cao, R., et al. (2011). Serum 27-nor-5 beta-Cholestane-3,7,12,24,25 pentol glucuronide discovered by metabolomics as potential diagnostic biomarker for epithelium ovarian cancer. *Journal of Proteome Research, 10*(5), 2625–2632.

Cui, Y., Kaisaierjiang, A., Cao, P., Wu, Z. Y., & Lv, Q. (2014). Association of apolipoprotein A5 genetic polymorphisms with steroid-induced osteonecrosis of femoral head in a Chinese Han population. *Diagnostic Pathology, 9*(1), 229.

da Silva, T. F., Sousa, V. F., Malheiro, A. R., & Brites, P. (2012). The importance of ether-phospholipids: A view from the perspective of mouse models. *Biochimica et Biophysica Acta—Molecular Basis of Disease, 1822*(9), 1501–1508.

El-Maraghy, S. A., & Mehana, N. A. (2015). Modulatory effects of L-arginine and soy enriched diet on bone homeostasis abnormalities in streptozotocin-induced diabetic rats. *Chemico-Biological Interactions, 229*(5), 9–16.

Frey, J. L., Li, Z., Ellis, J. M., et al. (2015). Wnt-lrp5 signaling regulates Fatty Acid metabolism in the osteoblast. *Molecular and Cellular Biology, 35*(11), 1979–1991.

Fukumoto, S., Iwamoto, T., Sakai, E., et al. (2006). Current topics in pharmacological research on bone metabolism: Osteoclast differentiation regulated by glycosphingolipids. *Journal of Pharmacological Sciences, 100*(3), 195–200.

Gangji, V., De Maertelaer, V., & Hauzeur, J. P. (2011). Autologous bone marrow cell implantation in the treatment of non-traumatic osteonecrosis of the femoral head: Five year follow-up of a prospective controlled study. *Bone, 49*(5), 1005–1009.

Ge, P., Cui, Y., Liu, F., Luan, J., Zhou, X., & Han, J. (2015). L-carnitine affects osteoblast differentiation in NIH3T3 fibroblasts by the IGF-1/PI3 K/Akt signalling pathway. *BioScience trends, 9*(1), 42–48.

Gertsman, I., Gangoiti, J. A., Barshop, B. A., et al. (2014). Validation of a dual LC-HRMS platform for clinical metabolic diagnosis in serum, bridging quantitative analysis and untargeted metabolomics. *Metabolomics: Official Journal of the Metabolomic Society, 10*(2), 312–323.

Gonzalez, E., van Liempd, S., Conde-Vancells, J., et al. (2012). Serum UPLC–MS/MS metabolic profiling in an experimental model for acute-liver injury reveals potential biomarkers for hepatotoxicity. *Metabolomics: Official Journal of the Metabolomic Society, 8*(6), 997–1011.

Hernigou, P., Flouzat-Lachaniette, C. H., Delambre, J., et al. (2015). Osteonecrosis repair with bone marrow cell therapies: State of the clinical art. *Bone, 70*, 102–109.

Holmes, E., Loo, R. L., Stamler, J., et al. (2008a). Human metabolic phenotype diversity and its association with diet and blood pressure. *Nature, 453*(7193), 396–401.

Holmes, E., Wilson, I. D., & Nicholson, J. K. (2008b). Metabolic Phenotyping in Health and Disease. *Cell, 134*(5), 714–717.

Jogl, G., & Tong, L. (2003). Crystal structure of carnitine acetyltransferase and implications for the catalytic mechanism and fatty acid transport. *Cell, 112*(1), 113–122.

Kang, P., Xie, X., Tan, Z., et al. (2015). Repairing defect and preventing collapse of femoral head in a steroid-induced osteonecrotic of femoral head animal model using strontium-doped calcium polyphosphate combined BM-MNCs. *Journal of Material Science, Material Medicine, 26*(2), 80.

Karner, C. M., Esen, E., Okunade, A. L., Patterson, B. W., & Long, F. (2015). Increased glutamine catabolism mediates bone anabolism in response to WNT signaling. *The Journal of Clinical Investigation, 125*(2), 551–562.

Lee, H. J., Choi, S. J., Hong, J. M., et al. (2009). Association of a Polymorphism in the Intron 7 of the SREBF1 Gene with Osteonecrosis of the Femoral Head in Koreans. *Annals of Human Genetics, 73*(1), 34–41.

Nada, M. A., Rhead, W. J., Sprecher, H., Schulz, H., & Roe, C. R. (1995). Evidence for Intermediate Channeling in Mitochondrial β-Oxidation. *The Journal of Biological Chemistry, 270*(2), 530–535.

O'Connor, E. M., Grealy, G., McCarthy, J., et al. (2015). Effect of phylloquinone (vitamin K1) supplementation for 12 months on the indices of vitamin K status and bone health in adult patients with Crohn's disease. *British Journal of Nutrition, 112*(7), 1163–1174.

Phang, J. M., Liu, W., & Zabirnyk, O. (2010). Proline Metabolism and Microenvironmental Stress. *Annual Review of Nutrition, 30*, 441–463.

Phang, J. M., Pandhare, J., & Liu, Y. (2008). The Metabolism of Proline as Microenvironmental Stress Substrate. *The Journal of nutrition., 138*(10), 2008S–2015S.

Priori, R., Scrivo, R., Brandt, J., et al. (2013). Metabolomics in rheumatic diseases: the potential of an emerging methodology for improved patient diagnosis, prognosis, and treatment efficacy. *Autoimmunity Reviews, 12*(10), 1022–1030.

Qi, X., & Zeng, Y. (2015). Biomarkers and pharmaceutical strategies in steroid-induced osteonecrosis of the femoral head: A literature review. *Journal of International Medical Research, 43*(1), 3–8.

Qiang, H., Liu, H., Ling, M., Wang, K., & Zhang, C. (2015). Early Steroid-Induced Osteonecrosis of Rabbit Femoral Head and Panax notoginseng Saponins: mechanism and Protective Effects. *Evidence-based Complementary and Alternative Medicine: eCAM,*. doi:10.1155/2015/719370.

Ragab, Y., Emad, Y., & Abou-Zeid, A. (2008). Bone marrow edema syndromes of the hip: mRI features in different hip disorders. *Clinical Rheumatology, 27*(4), 475–482.

Sauer, A. V., Mrak, E., Jofra, H. R., et al. (2009). ADA-deficient SCID is associated with a specific microenvironment and bone phenotype characterized by RANKL/OPG imbalance and osteoblast insufficiency. *Blood, 114*(15), 3216–3226.

Seamon, J., Keller, T., Saleh, J., & Cui, Q. (2012). The pathogenesis of nontraumatic osteonecrosis. *Arthritis,*. doi:10.1155/2012/601763.

Shea, M. K., Kritchevsky, S. B., Hsu, F. C., et al. (2015). Health ABC Study, The association between vitamin K status and knee osteoarthritis features in older adults: the Health, Aging and Body Composition Study. *Osteoarthritis and Cartilage, 23*(3), 370–378.

Shi, B., Li, G., Wang, P., et al. (2010). Effect of antler extract on corticosteroid-induced avascular necrosis of the femoral head in rats. *Journal of Ethnopharmacology, 127*(1), 124–129.

Shih, L. Y., Wong, Y. C., & Shih, H. N. (2009). One-stage hip arthroplasty and bone grafting for bilateral femoral head osteonecrosis. *Clinical Orthopaedics and Related Research, 467*(6), 1522–1528.

Smith, R. J., Reddi, A. H., & Phang, J. M. (1979). Changes in proline synthetic and degradative enzymes during matrix-induced cartilage and bone formation. *Calcified Tissue International, 27*(3), 275–279.

Song, B. C., Joo, N. S., Aldini, G., & Yeum, K. J. (2014). Biological functions of histidine-dipeptides and metabolic syndrome. *Nutrition Research and Practice, 8*(1), 3–10.

Sreekumar, A., Poisson, L. M., Rajendiran, T. M., et al. (2009). Metabolomic profiles delineate potential role for sarcosine in prostate cancer progression. *Nature, 457*(7231), 910–914.

Sutton-McDowall, M. L., Purdey, M., Brown, H. M., et al. (2015). Redox and anti-oxidant state within cattle oocytes following in vitro maturation with bone morphogenetic protein 15 and follicle stimulating hormone. *Molecular Reproduction and Development, 82*(4), 281–294.

Tadaishi, M., Nishide, Y., Tousen, Y., Kruger, M. C., & Ishimi, Y. (2014). Cooperative effects of soy isoflavones and carotenoids on osteoclast formation. *Journal of Clinical Biochemistry and Nutrition, 54*(2), 109–115.

Tingart, M., Beckmann, J., Opolka, A., et al. (2009). Analysis of Bone Matrix Composition and Trabecular Microarchitecture of the Femoral Metaphysis in Patients with Osteonecrosis of the Femoral Head. *Orthopaedic Research Society, 27*(9), 1175–1181.

van der Gulik, P. T., & Speijer, D. (2015). How amino acids and peptides shaped the RNA world. *Life, 5*(1), 230–246.

Van Wietmarschen, H. A., Dai, W., van der Kooij, A. J., et al. (2012). Characterization of rheumatoid arthritis subtypes using symptom profiles, clinical chemistry and metabolomics measurements. *PLoS One, 7*(9), e44331.

Wen, Q., Ma, L., Chen, Y. P., Yang, L., Luo, W., & Wang, X. N. (2008). Treatment of avascular necrosis of the femoral head by hepatocyte growth factor-transgenic bone marrow stromal stem cells. *Gene Therapy, 15*(23), 1523–1535.

Wu, R. W., Wang, F. S., Ko, J. Y., Wang, C. J., & Wu, S. L. (2008). Comparative serum proteome expression of osteonecrosis of the femoral head in adults. *Bone, 43*(3), 561–566.

Xie, H., Yang, B., Zhou, X., et al. (2010). L-carnitine and taurine synergistically inhibit the proliferation and osteoblastic differentiation of vascular smooth muscle cells. *Acta Pharmacologica Sinica, 31*(3), 289–296.

Yamaguchi, M. (2012). Role of carotenoid β-cryptoxanthin in bone Homeostasis. *Journal of Biomedical Science,*. doi:10.1186/1423-0127-19-36.

Yamaguchi, M., & Weitzmann, M. N. (2009). The bone anabolic carotenoids p-hydroxycinnamic acid and β-cryptoxanthin antagonize NF-κB activation in MC3T3 preosteoblasts. *Molecular Medicine Reports, 2*(4), 641–644.

Yin, J. M., Zhao, L., Zhao, S. C., Guo, Y. J., Liu, Z. T., & Liu, Z. T. (2014). Relationship between the Apolipoprotein AI, B gene polymorphism and the risk of non-traumatic osteonecrosis. *Lipids Health Dis, 13*(1), 149. doi:10.1186/1476-511X-13-149.